Engineering Structures 278 (2023) 115492

Contents lists available at ScienceDirect

Engineering Structures

journal homepage: www.elsevier.com/locate/engstruct

Analysis and prediction of masonry wallette strength under combined compression-bending via stochastic computational modeling

Semih Gonen [a,*], Bora Pulatsu [b], Paulo B. Lourenço [c], José V. Lemos [d], Kagan Tuncay [e], Emrah Erduran [a]

[a] Oslo Metropolitan University, Oslo, Norway
[b] Carleton University, Ottawa, ON, Canada
[c] University of Minho, Guimarães, Portugal
[d] LNEC, Lisbon, Portugal
[e] Middle East Technical University, Ankara, Turkey

ARTICLE INFO

Keywords:
Spatial stochastic analysis
Uncertainty quantification
Masonry strength prediction
DEM
Computational modeling
Contact mechanics

ABSTRACT

The out-of-plane flexural bending capacity of masonry is a fundamental property for understanding the behavior of masonry structures. This study investigates the behavior of unreinforced masonry wallettes subjected to combined compression-flexural loading using the discrete element method (DEM), and provides a novel framework to estimate the masonry strength. A simplified micro-modeling strategy is utilized to analyze a masonry wallette, including the variation of the mechanical properties in masonry units and joints. Stochastic DEM analyses are performed to simulate brickwork assemblages, assuming a *strong unit-weak joint* material model typical of most masonry buildings, including historical ones. Once the proposed computational approach is validated against the experimental findings, the effect of spatial and non-spatial variation of mechanical properties is explored. Two failure types are identified: *joint failure* and *brick failure*. For each failure mechanism, the variability of the response and the effects of the modeling parameters on the load-carrying capacity is quantified. Afterward, Lasso regression is employed to determine predictive equations in terms of the material properties and vertical pressure on the wallette. The results show that the most important parameters changing the response are the joint tensile strength and the amount of vertical stress for *joint failure*, whereas the unit tensile strength dominates the response for *brick failure*. Overall, this research proposes a novel framework adopting validated advanced computational models that feed on simple test results to generate data that is further utilized for training response prediction models for complex structures.

1. Introduction

Masonry structures constitute a vast majority of residential and historical buildings worldwide. The workmanship, such as the morphology of the wall cross-sections, arches, etc., and the material used in the masonry construction reveal substantial differences in different regions of the world as this type of construction relies heavily on the local-construction culture and available resources [1,2]. Typically, this widespread construction technique consists of units, such as clay brick, stone blocks, adobe, and a binding material, *e.g.*, cement or lime-based mortar, where each constituent has different mechanical properties. On the other hand, composite material characteristics of masonry are influenced by the mortar, unit, and unit-mortar-interface properties and their mechanical interaction. The considerable difference in stiffness and strength parameters of masonry unit and mortar joints yields weak planes at the interfaces where cracking and sliding failures are likely to occur, so-called strong unit-weak joint (*SU-WJ*) action. However, it is also possible to obtain a weak unit-strong joint (*WU-SJ*) response, where considerable damage is found in masonry units, primarily because of incompatible selection of mortar-type (stiffer and stronger than the units) or highly deteriorated/damaged bricks or blocks [3,4]. In both cases, the overall fracture pattern, deformability, and strength of masonry are controlled by the distinct features and mechanical interaction among the units and mortar joints.

Various computational modeling strategies have been proposed in the last three decades to better understand the complex fracture

* Corresponding author.
E-mail address: semihgon@oslomet.no (S. Gonen).

https://doi.org/10.1016/j.engstruct.2022.115492
Received 26 September 2022; Received in revised form 6 December 2022; Accepted 14 December 2022
Available online 23 December 2022

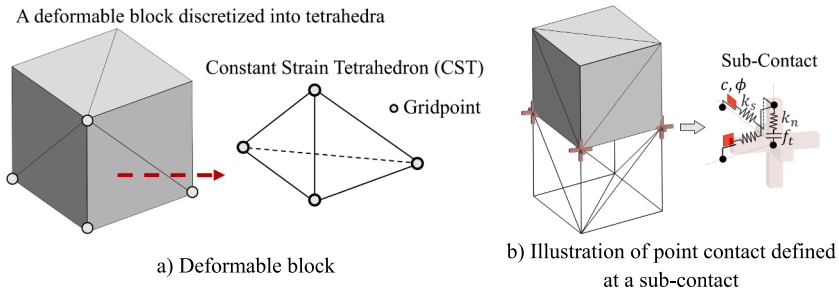

Fig. 1. A deformable block and point-contact representation.

mechanism of masonry and the mechanics of masonry structures [5]. These strategies can be categorized as continuum and discontinuum-based solutions. The former technique represents the composite nature of masonry as a homogenous isotropic or orthotropic medium considering plasticity or other macro-scale constitutive laws (referred to as macro-modeling) [6–10]. The damage is smeared through the continuous medium since no distinction between the units and mortar is made. The latter approach, called micro-modeling, implements the discontinuities (displacement jumps) and mechanically interacting rigid/deformable bodies in the numerical formulation [11]. The discontinuous finite element analysis (D-FEA) and the discrete element method (DEM) are the most common techniques used in micro-modeling [12–23]. Although the discontinuum models offer a detailed representation of inherent characteristics of the masonry and its mechanical behavior compared to the conventional continuum models, their computational demand and a large number of required input parameters prevent their widespread use.

The mechanical properties of each constituent of the masonry often differ spatially, which may yield significant variation in the macro and mesoscale strength parameters of masonry. In this respect, probabilistic modeling of masonry structures has gained more attention in the last decades due to its promising features, such as explicitly considering the uncertainties in modeling parameters, quantifying the variability of the structural response, and the propagation of parameter uncertainties into response variables. Masonry units [3], structural components like masonry walls [24–30], pier-spandrel systems [31–33], buildings [34–36], and bridges [37–39] have been investigated using probabilistic assessment. However, there is still a limited number of studies in the literature compared to their deterministic counterparts. This gap is especially prevalent for masonry units and small-scale assemblages like masonry prisms and wallettes. Experimental investigations testing the effect of *SU-WJ* and *WU-SJ* behavior on the macro-response of masonry under various load patterns, such as direct tension parallel to bed joints, combined compression-bending, or tension-bending, are limited in the literature. On the other hand, numerical investigations studying this phenomenon [3,40,41] have become more available without considering the associated uncertainties.

2. Research motivation, novelty, and methodology

There is a need for further experimental and analytical research, especially when the complex behavior of masonry subjected to the combined actions of compression, bending, shear, or torsion is considered. This need is amplified for detailed computational models considering uncertainty in the parameters and their spatial variation. One type of behavior where joint actions are observed is the horizontal bending of masonry, commonly observed in the out-of-plane behavior of masonry piers and spandrels. Horizontal bending can show complex behavior, including combined tension, shear, and torsion at the joints. The horizontal bending strength, *i.e.*, one-way out-of-plane flexural bending capacity of masonry, is a fundamental parameter for masonry design [42–44] and will be addressed in this study.

The application of advanced statistical models, such as machine learning algorithms, in the structural assessment of masonry constructions is limited due to the lack of data. Amongst a few examples, most research is dedicated to predicting masonry compressive strength [45–50], partly because masonry compression experiments are the most widespread. The database of masonry tests has been growing significantly. However, it is not feasible to test all possible combinations, given the large variability of the masonry properties [45]. Also, challenges related to the data quality and heterogeneity of the database continue to exist [51]. To this end, two research questions lay the foundation of this research: (i) *How can we improve our knowledge and predictive models for masonry structures in addition to extensive testing? (ii) Can response data be generated by leveraging less complicated and inexpensive tests?*

In the context of these general questions, this research aims to contribute to the understanding of masonry behavior, specifically under horizontal bending. We present and motivate a novel idea that adopts advanced computational modeling, which feeds on inexpensive and simple test results, to generate data for training response prediction models for more complicated structures. To this end, we first aim to accurately model the horizontal bending behavior of masonry wallettes. Discontinuum models are utilized and validated by comparing the predicted and observed responses. The discrete element method (DEM) [52] is used to simulate the composite behavior of brickwork assemblages based on the simplified micro-modeling strategy [53]. A masonry wallette is analyzed by explicitly representing the units and unit-mortar interfaces to address the combination of *SU-WJ*, which is typical for most masonry buildings, including historic masonry constructions. Elasto-plastic blocks are adopted to replicate the masonry units, and mortar joints are prescribed as zero-thickness interfaces.

Once the proposed modeling approach is validated against experimental findings presented in the literature, stochastic analyses are performed on masonry wallettes to quantify the effects of the variability of modeling parameters on the overall behavior and load-bearing capacity. The uncertainty in the masonry properties is considered by explicitly taking into account the variation in the elasticity modulus and tensile strength of brick units and the joint tensile strength and friction angle of masonry. The effect of vertical pressure on masonry behavior is also considered by employing five different pre-compression stress levels. In stochastic analyses, a total of 1000 sets of parameters are generated, and computations are conducted for each set. In half of the analysis, the mechanical properties of the masonry are assumed to be spatially constant (*i.e.*, no spatial variation of material properties). In the remaining half, the spatial variation of the joint and unit properties for each wallet is considered, and the effects of spatial variation on the wallette's behavior are evaluated.

Finally, using the dataset created by the numerical analysis, predictive equations to estimate the load-bearing capacity of the wallettes are developed and compared with experimental results from the literature to test the prediction models. Using the presented approach (numerical and predictive models) in conjunction with experimental results, this study targets to alleviate broad and costly experimental campaigns and to improve the predictive equations provided by

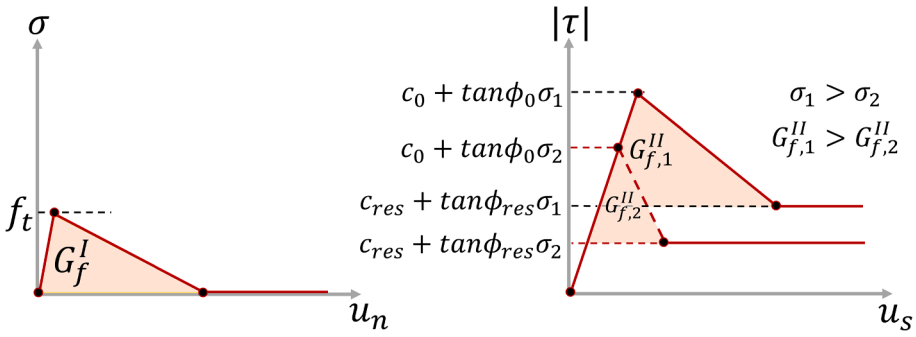

Fig. 2. Contact constitutive laws in the normal and shear directions: tension (left) and shear (right).

guidelines and standards.

3. Computational background of DEM: deformable blocks

To be able to realistically simulate the behavior of small-scale stone or brickwork assemblages (*e.g.,* prisms and wallettes) under complex loading, it is essential to explicitly consider masonry units and mortar joints in the numerical formulation. The detailed representation of masonry texture provides an accurate prediction of the capacity and a better understanding of the fracture mechanisms in composite structures of masonry. Furthermore, inherent material uncertainty, both spatial and non-spatial, can be addressed.

In the present research, the masonry wallette is represented by a group of deformable polyhedra in a discontinuum-based setting where each masonry unit is expanded up to the half-thickness of the mortar joints so that units are simulated as rectangular continuum blocks, whereas mortar joints are represented by zero-thickness interfaces. Hence, unlike methods tailored for continua (*e.g.*, standard finite element analysis), no continuity is sought between the pre-defined blocks, which can independently rotate, slide or displace, relying on the surrounding forces within the discontinuous system. The action/reaction forces developing between the adjacent blocks are obtained using orthogonal springs (k_n, k_s) defined at the sub-contact points along the contact surface; see Fig. 1.

The deformability of discrete blocks is introduced by discretizing them into constant strain tetrahedra (internal three-dimensional mesh), as shown in Fig. 1a, where the vertices are denoted as gridpoints (nodes). The motion of a deformable discrete block is computed based on Newton's second law, which is applied for each gridpoint defined within the block domain. The governing differential equations are solved numerically via explicit finite difference formulation, where Cundall's local non-viscous damping is adopted to obtain quasi-static solutions efficiently [54]. In Equation 1, the central difference solution of the equations of motion for a gridpoint is presented. Note that the new velocities ($\dot{u}_i^{t+\Delta t/2}$) are calculated at the mid-intervals of the time step (Δt).

$$\dot{u}_i^{t+\frac{\Delta t}{2}} = \dot{u}_i^{t-\frac{\Delta t}{2}} + \frac{\Delta t}{m}\left(\Sigma F_i^t - \alpha\left|\Sigma F_i^t\right| sgn\left(\dot{u}_i^{t-\frac{\Delta t}{2}}\right)\right) \tag{1}$$

Here, ΣF_i, m and α are the summation of force vectors (also referred to as nodal unbalanced force), gridpoint (nodal) mass representing the sum of mass contributions from all tetrahedra having the gridpoint in common, and non-dimensional damping constant which is typically set to 0.8 for fast convergence [54]. Also, $sgn(\bullet)$ is the sign function, which imposes the following condition: $sgn(\xi) = 1$, *if* $\xi \geq 0$; $sgn(\xi) = -1$, *if* $\xi < 0$. The total force vector includes external forces, sub-contact forces (only for gridpoints prescribed at the block surface), body forces due to gravity, and the contribution of the internal stresses in the tetrahedral elements adjacent to the gridpoint. The obtained nodal velocities are then utilized to update block positions and calculate the relative contact displacements employed to determine contact forces. The gridpoint displacements can then be obtained using Equation 2. Typically, the Coulomb-Slip joint model with tension cut-off is utilized in the literature to simulate the mechanical behavior at the contact points, which requires initial and residual cohesion (c_0, c_{res}), friction angle (ϕ_0, ϕ_{res}), and tensile strength (f_t). Although the standard/simple contact models provide an acceptable compromise between accuracy and required input parameters, they may yield significant underestimation and severe local instabilities in the solutions, as demonstrated in [55]. Once the contact forces are obtained, they are utilized in the equations of motion to calculate new gridpoint velocities.

$$u_i^{t+\frac{\Delta t}{2}} = u_i^{t-\frac{\Delta t}{2}} + \left(\dot{u}_i^{t+\frac{\Delta t}{2}}\right)\Delta t \tag{2}$$

Failure within the blocks (consisting of constant strain tetrahedral (CST) elements) is simulated using the elasto-plastic material model. Based on the known velocity field, the incremental components of the strain tensor ($\Delta\varepsilon_{ij}$) can be derived from each CST as follows:

$$\Delta\varepsilon_{ij} = \frac{\Delta t}{2}\left(\frac{\partial \dot{u}_i}{\partial x_j} + \frac{\partial \dot{u}_j}{\partial x_i}\right) \tag{3}$$

The mixed discretization technique is adopted to avoid any mesh-locking response due to CST elements and provide more volumetric flexibility, as detailed in [56,57]. An incremental numerical algorithm is used to compute and update the new stress state for each CST corresponding to the time at $t + \Delta t$. Note that the nonlinear material model is simulated within the framework of an explicit solution scheme in DEM by relying on predictor (elastic guess) and corrector procedure to update the stress state based on the Mohr-Coulomb failure criteria. Specifically, at each time step principle elastic strain increments ($\Delta e_i^{elastic}$) are obtained to get principle stress increments ($\Delta\sigma_i$) that is computed by substructing the plastic strain ($\Delta e_i^{plastic}$) from total increments (Δe_i) based on the plasticity theory. Then, the new stress state ($\sigma_i^{t+\Delta t}$) is obtained by adding the computed stress increment to the previous one (σ_i^t) and is updated according to the prescribed failure criterion. Therefore, the initial elastic guess is replaced by plastic corrections in case the failure criterion is violated, and the new stress state is updated by mapping it back to the yield surface. It is also important to note that a perfectly-plastic non-associated flow rule for shear and a softening associated flow rule for tensile failure is adopted during the analyses. The readers are referred to [58] for further details. Throughout this research, a commercial three-dimensional discrete element code, 3DEC, developed by ITASCA, is used, in which the explained elasto-plastic constitutive model for blocks is readily provided. However, instead of using standard brittle contact models mentioned earlier, coupled fracture energy-based contact constitutive laws, recently implemented by the authors [59], are adopted to better capture the material behavior at the mesoscale. It is worth noting that the adopted contact models do not include any stiffness degradation in the unloading regime, which makes them applicable to pushover types of analysis in line with the scope of this study (*e.g.*,

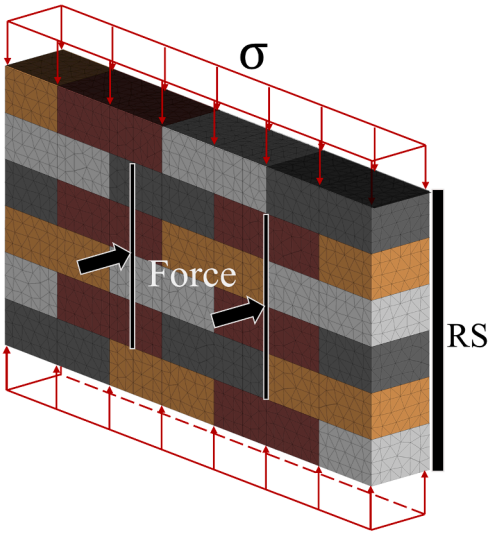

Fig. 3. Illustration of the reference study, including the loading and boundary conditions, **RS**: Roller Support – brickwork wallette subjected to combined vertical stress and horizontal bending.

Table 1
Masonry unit (block) and joint properties used in the discontinuum model.

E_b(GPa)	$\nu(-)$	$f_{t,u}$(MPa)	c_u(MPa)	$G^I_{f,u}$(N/m)
15	0.2	3.75	1.5 f_t	100
k_n, k_s(GPa/m)	f_{tj}, c_j(MPa)	ϕ_0, ϕ_{res}(°)	G^I_{fj}(N/m)	G^{II}_{fj}(N/m)
165, 0.4 k_n	0.30, 0.36	35, 35	9	10 G^I_{fj}

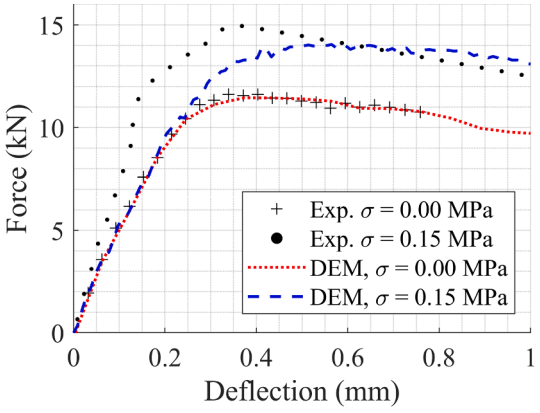

Fig. 4. Force-deflection curves: Comparison between experimental results [61] and proposed DEM-based analysis.

monotonic loading instead of cyclic).

Since the primary motivation of this research is to explore the out-of-plane response of masonry wallettes, only tensile and shear failure modes at the joints are considered. The proposed contact models are shown in Fig. 2, where linear softening branches are defined for post-peak regimes controlled by the mode-I and II fracture energies (G^I_f, G^{II}_f) once the contact stresses go beyond the peak stresses. It is worth noting that the relative contact displacements in normal (u_n) and shear (u_s) directions are utilized in contact stress-displacement laws that are later converted to forces by multiplying them with the assigned contact area. Similar to deformable blocks, a contact stress update routine is executed based on the proposed contact models, where, at each step, the computed contact stresses are corrected (if applicable) according to the defined failure criteria; see Fig. 2. The adopted contact model is written in C++ and compiled as a dynamic link library (DLL) into 3DEC software using the user-defined constitutive model option.

Thus, a dynamic computation cycle is run in the pseudo-time domain. Note that the explicit numerical procedure of DEM provides a conditionally stable solution. As a result, it requires limitations in the timestep to satisfy the stability criterion for the computation of inter-block relative displacement and internal block deformation. To ensure numerical stability, a sufficiently small-time step less than the critical time step, Δt_c (Equation 3) is adopted.

$$\Delta t_c = 2\sqrt{\frac{m}{k_{gp}}} \tag{4}$$

where k_{gp} represents the nodal stiffness obtained by adding zone and contact (only the gridpoint on the faces) stiffness [60].

In the next section, validation of the proposed modeling strategy is presented by comparing it with the experimental results.

4. Validation: deterministic analysis

The horizontal bending strength, *i.e.*, one-way out-of-plane (OOP) flexural bending capacity, is a fundamental parameter for masonry wall design [42]. This type of behavior is commonly observed in the seismic behavior of perforated walls. Compared to a one-way vertical bending associated with a bed-joint failure, horizontal bending usually displays a complex torsion-shear interaction at unit-mortar interfaces. Moreover, the confining action of the vertical stress can increase the torsional resistance developing at the bed joints [42]. To explore this phenomenon, Willis et al. [61] performed a comprehensive testing campaign using unreinforced masonry wallettes with clay brick dimensions of 230 × 65 × 114 mm^3 (length × height × width) and 10 mm thickness of mortar joints. The reference experiment is utilized as a benchmark study in this section. The illustration of the test setup, including loading and boundary conditions, is shown in Fig. 3. The adopted mechanical properties for blocks and joints are given in Table 1. The readers are referred to Willis et al. [61] for detailed information about the experiment.

The experimental and numerical results are presented in Fig. 4, where the vertical compressive stress is set to σ = 0 and σ = 0.15 MPa and applied prior to the horizontal load. As can be seen from the results (Fig. 4), the proposed modeling approach predicts well the ultimate load capacity of the wallette as well as its initial stiffness and post-peak behavior. In this regard, it is worth noting that the employed contact constitutive law uses constant stiffness (k_n, k_s) which is independent of the vertical pressure (or normal stress). However, the stiffness of masonry-like materials may be affected by the vertical pressure and, for dry-stacked masonry, shows a nonlinear trend even in the linear elastic regime, demonstrated and discussed in [62]. This phenomenon can also be noticed in Fig. 4, where a higher initial stiffness was obtained in the reference study, even if more tests would be needed to confirm this result. Despite this, a good overall match is obtained between the experimental results and the proposed discontinuum-based modeling strategy, which will be further utilized for stochastic analysis in the following section.

5. Flexural behavior of masonry wallette: stochastic analyses

The mechanical properties of masonry structures are probabilistic due to the inherent variability in masonry constituents, the construction features, and the uneven degradation of the material [63]. Furthermore, the loading and boundary conditions, which can significantly affect and alter structural behavior and capacity, contribute to the uncertainty. To this end, stochastic models provide more realistic solutions for structural engineering problems [64]. As mentioned earlier, these uncertainties have been recognized by the research community, and probabilistic

Table 2
Information for Strong Unit - Weak Joint Combination.

Random Variable	Probability Distribution	Mean (μ)	Coefficient of Variation (COV)
$f_{t,j}$(MPa)	Lognormal	0.3	0.40
$f_{t,u}$(MPa)	Lognormal	3.75	0.25
ϕ_j(°)	Normal	35	0.10
E_b(MPa)	Lognormal	15,000	0.30
Dependent Variable	**Relationship**		
c_j	$1.2f_{t,j}$		
$G^I_{f,j}$	$0.03f_{t,j}$		
$G^{II}_{f,j}$	$10G^I_{f,j}$		
c_u	$1.5f_{t,u}$		
$G^I_{f,u}$	$0.04f^{0.7}_{t,u}$		
k_n	$\frac{E_b \times E_m}{t \times (E_b - E_m)}$		

t: Mortar joints thickness (0.01 m), E_m: Mortar elastic modulus ($\approx 0.1E_b$)

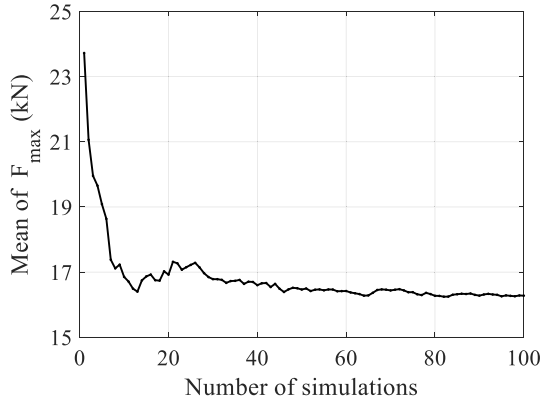

Fig. 5. Example of the average maximum force vs. the number of simulations (vertical stress of 0.50 MPa).

assessment of masonry structures has recently been employed for various structural typologies [24,29–31,34,37]. While such studies showed the importance of stochastic modeling in predicting the behavior and capacity of masonry, they also demonstrated a further need for quantifying the uncertainties included in the analysis.

5.1. Sampling of the model parameters

In the probabilistic analysis approach, the unit and joint properties are considered deterministic, random, or dependent variables. The most sensitive parameters associated with the strength of masonry wallettes are designated as random variables. Moreover, the parameters indicating significant variations based on the experimental findings are also taken as random variables. As such, throughout this study, the joint (or bond) tensile strength ($f_{t,j}$), the unit (brick) tensile strength ($f_{t,u}$), the joint friction angle (ϕ), and the elasticity modulus of masonry units (E_b) are considered random variables in the stochastic analysis. Furthermore, the cohesion of the bricks and joints are defined as variables dependent on the unit ($f_{t,u}$) and joint tensile strength ($f_{t,j}$), respectively, using the following relationships: $c_u = 1.5f_{t,u}$ and $c_j = 1.2f_{t,j}$. Similarly, the mode-I and II fracture energies (G^I_f and G^{II}_f) are calculated based on the strength values suggested in [65,66]; hence, they are treated as dependent variables. Moreover, other relationships are adopted based on the recommendations given in the literature [67]. In Table 2, both random and dependent variables are presented.

A probability distribution is assigned to each random variable for the sampling process. The unit and joint tensile strength and the elasticity modulus of bricks follow a lognormal distribution to prevent negative values during sampling, similar to the related literature [34,68]. The normal distribution is utilized for the joint friction angle [3,24]. The mean and the coefficient of variation (COV) of the tensile strength of units are obtained from experimental results [69]. The COV of the joint tensile strength is determined as 0.40 based on the highly scattered test results [42,70].

The data sampling is performed after defining the probability distributions for the random variables. The Latin Hypercube Sampling (LHS) method [71] is used to derive the sample values from each probability distribution. It is assumed that a 50% correlation exists between E_b and $f_{t,u}$ in order to prevent unrealistic cases of high brick tensile strength accompanied by very low elasticity modulus. No other correlation is defined between the random variables. Note that the sampling procedure is slightly different for the non-spatial and spatial stochastic analyses. For the non-spatial analysis, where the spatial variation of the variables is not considered, 100 sample values are generated for each random variable to be used in the simulations. In every Monte Carlo simulation, each parameter has a single value that is uniform over the entire structure. Therefore, each of the 100 sample values of a variable is being used in 100 different simulations of the wallette response. Five vertical pre-compression stress levels are considered in the analyses: 0, 0.075, 0.15, 0.25, and 0.50 MPa. The same 100 samples are used in every loading scenario, resulting in 500 simulations. The number of simulations is determined by observing the change in the average maximum force obtained from the analyses. For instance, Fig. 5 displays the variation in the mean of the maximum force with an increasing number of analyses when the vertical stress is 0.50 MPa, and the variation in the mean maximum force stabilizes after approximately 80 simulations. Therefore, a minimum of 100 analyses can be considered to sufficiently represent the variation in the obtained maximum force for each set of analyses.

For the spatial stochastic analysis, the parameter values are defined as variables adopting the following approach. First, an identification number is defined separately for each joint (or contact plane) and masonry unit in the discrete block system, as shown in Fig. 6. There are 24 masonry units and 38 joints considered. Using the prescribed distributions given in Table 2 and LHS, different tensile strength and elasticity modulus values are assigned to each of the 24 masonry units, whereas different bond tensile strength and friction angle values are assigned to each joint. Therefore, in each of the 100 simulations, 24 brick properties, and 38 bond properties are sampled. Similar to the non-spatial analyses, the identical vertical stress levels are considered using the same parameter values at the units and joints; hence, a total of 500 simulations are conducted.

5.2. Non-spatial analysis

This section summarizes the results of the numerical analysis where the spatial variation in the random variables is ignored, *i.e.*, where the value of each random variable is constant throughout the entire wall. As a result of the numerical analysis, the wallettes displayed two distinct failure types, referred to as "*brick failure*" and "*joint failure*" hereafter. Joint failure is denoted as the separation and/or sliding displacement of contacts, whereas brick failure refers to the cracking of bricks accompanied by joint failure. Fig. 7 illustrates an example of each failure pattern. It is worth noting that these two cases are separated using an automated code-based procedure. Specifically, the results of computational models are grouped by monitoring the plastic strains associated with the tensile damage in bricks representing the cracking failure in masonry units. A similar force–displacement graph is observed for brick and joint failures within each group. For example, the joint failures have a smooth plateau or a descending branch after the inelastic behavior starts, but the brick failure shows a more complex behavior with stress drop(s) due to cracking in the units. The force–displacement curves separated for each failure pattern at different vertical pressure levels are

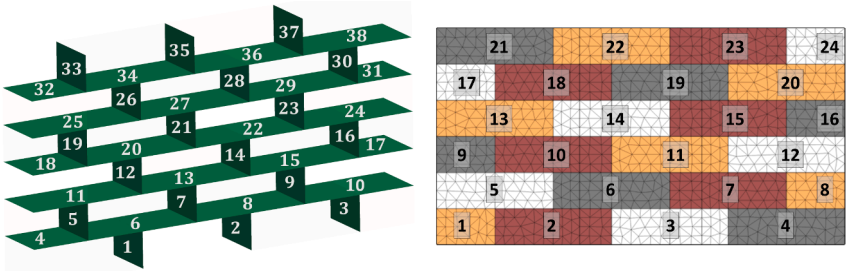

Fig. 6. Numbering (a) contact surface for joints and (b) masonry units.

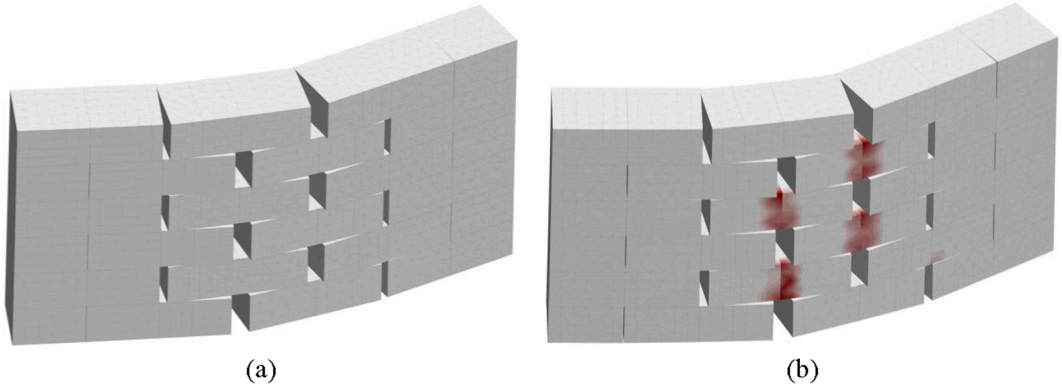

Fig. 7. Fracture mechanism obtained from the computational model: (a) joint (b) brick failure.

Table 3
Summary of the results - non-spatial analysis.

	F_{max} (kN)					
	Joint Failure		Brick Failure		All Data	
Vertical Pressure (MPa)	Mean	COV	Mean	COV	Mean	COV
0	10.84	0.30	13.59	0.22	11.17	0.30
0.075	11.72	0.25	14.43	0.26	12.15	0.27
0.15	12.76	0.23	14.58	0.22	13.20	0.23
0.25	14.17	0.21	14.99	0.19	14.49	0.20
0.50	17.83	0.14	15.86	0.19	16.28	0.18

given in Appendix (Fig. 15).

The results also highlight the prominent effect of the vertical stress on the OOP loading capacity of the masonry wallettes, see Table 3. With the increasing vertical stress, the maximum load capacity increases significantly. It is noted that the increase is more substantial for the joint failure than the brick failure since the cohesive bond strength at the horizontal joints increases with the normal stress, leading to a delay in the failure in the joint and resulting in higher load-bearing capacity. The mean load capacity increased by 64.5% and 16.7% for joint and brick failures, respectively, when the normal stress is increased from null to 0.5 MPa. On the other hand, the variability of the load capacity decreases considerably for the joint failure mode with an increase in the normal compressive stress, as indicated in Table 3 with the associated

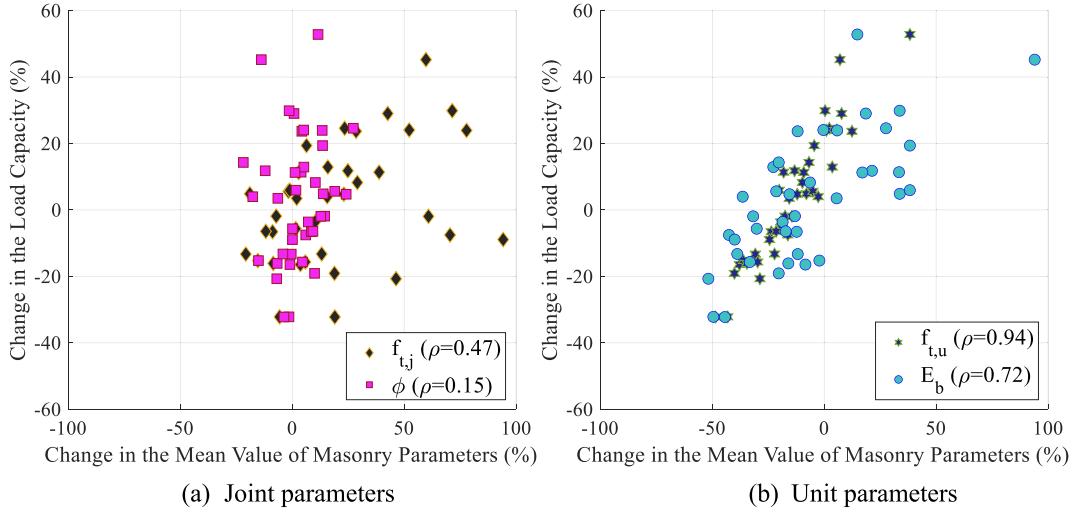

Fig. 8. Influence of the parameters on the OOP load capacity of wallettes (Brick failure, σ_v=0.25 MPa).

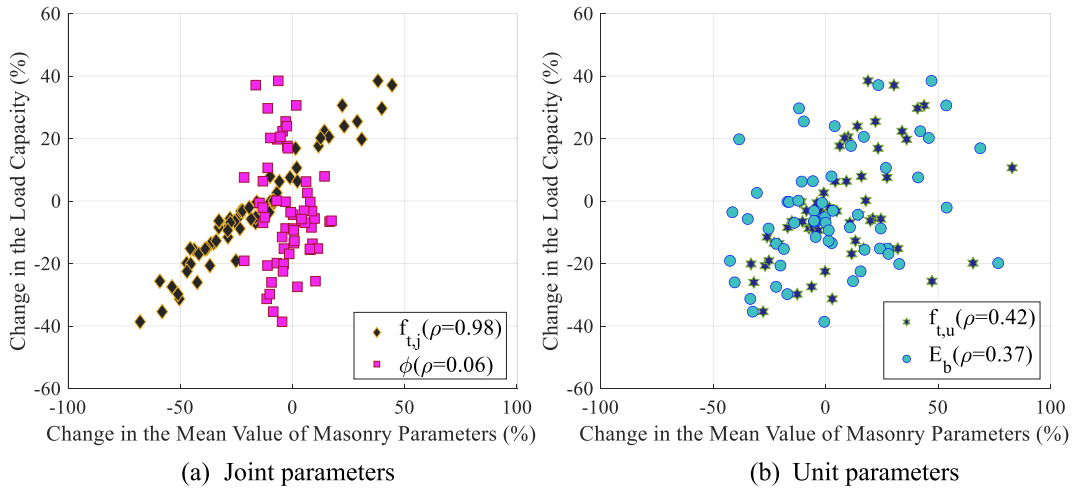

Fig. 9. Influence of the parameters on the OOP load capacity of wallettes (Joint failure, σ_v=0.25 MPa).

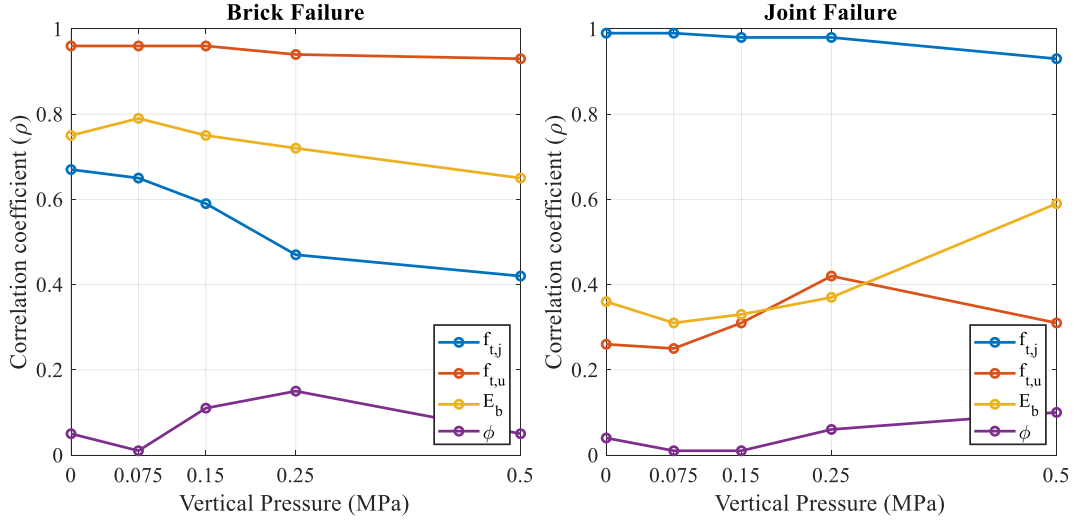

Fig. 10. Change of the correlation coefficient values with respect to the vertical pressure: (Left) brick failure, (Right) joint failure.

COV values. As can be seen, the COV decreases from 30% to 18% when all data are considered. The decrease is even more paramount for joint failure, whereas brick failure indicates a minor change in terms of capacity and its COV.

Additionally, the influence of the material properties on the ultimate load is investigated for both failure modes by inspecting the correlation between the material properties and the load-carrying capacity. Here, the degree of correlation is represented by Pearson product-moment correlation coefficient, $\rho_{x,y}$, given in Equation 4. The correlation coefficient quantifies a linear statistical dependence between two random variables (x, y) and ranges between 0 and 1, indicating zero and full correlation, respectively.

$$\rho_{x,y} = \frac{\Sigma(x_i - \bar{x})(y_i - \bar{y})}{\sqrt{\Sigma(x_i - \bar{x})^2 (y_i - \bar{y})^2}} \tag{4}$$

Fig. 8 and Fig. 9 illustrate the effect of the variables on the OOP load-carrying capacity of wallettes for the vertical stress of 0.25 MPa, for brick and joint failure, respectively. Further presented in the legend of Fig. 8 and Fig. 9 is the correlation of each parameter with the lateral load-carrying capacity computed using Equation 4. Specifically, a strong correlation is noted between the masonry unit parameters and the load-carrying capacity for the brick failure mode (Fig. 8), as expected. Moreover, a 98% linear correlation is found between the joint tensile strength (note that this property is also linked to the joint cohesion) and the load capacity in joint failure mode; see Fig. 9. These figures also display how the considered variables change concerning their mean values for each failure mode. For example, in Fig. 8 for the *brick failure*, it is observed that the joint tensile strength ($f_{t,j}$) values are often higher than their mean values, as indicated by the majority of the points being on the right hand side of the zero line, which means that the higher joint strength is more likely to be associated with brick failures.

The correlation of the load-carrying capacity of the wall with each of the random variables considered in the stochastic analysis is presented in Fig. 10 for different levels of vertical stress. This quantifies the effect of each modeling parameter on the wallette OOP load-carrying capacity. For the brick failure mode, the capacity of the wallette is strongly correlated, unsurprisingly and above 90%, with the brick tensile strength ($f_{t,u}$). A physically meaningful correlation between the capacity and elasticity modulus of bricks (E_b) is also observed (between 65 and 80%). It is also interesting to observe that, for the brick failure mode, the correlation between the capacity of wallettes and the joint tensile strength ($f_{t,j}$) or the elastic modulus of bricks decrease with increasing vertical stress. In terms of joint failures, the wallette strength is almost directly correlated with the joint tensile strength for low vertical stresses. With the increasing normal stresses, the effect of the joint friction angle (ϕ) on the load carrying capacity of the wallette increases.

Table 4
Summary of the results - spatial analysis.

	F_{max} (kN)					
	Joint Failure		Brick Failure		All Data	
Vertical Pressure (MPa)	Mean	COV	Mean	COV	Mean	COV
0	10.97	0.06	11.38	0.04	11.05	0.06
0.075	12.14	0.06	12.15	0.05	12.14	0.05
0.15	13.44	0.06	13.00	0.06	13.26	0.06
0.25	15.29	0.05	14.04	0.08	14.57	0.08
0.50	20.62	0.04	15.97	0.13	16.21	0.14

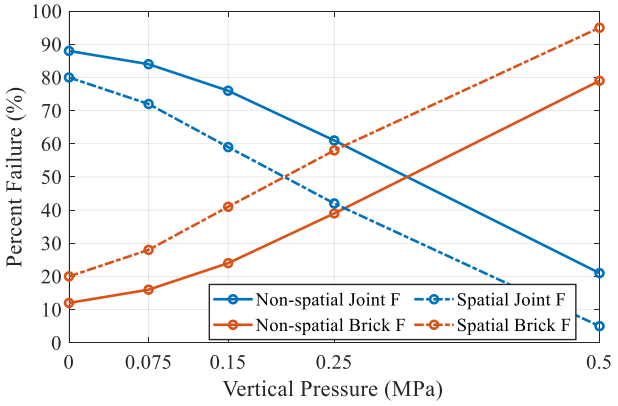

Fig. 11. Percentage of the failure modes vs. the vertical pressure levels.

Similarly, the correlation coefficient between the E_b and wallette strength increases because higher values of brick elasticity modulus cause joint failures, which at the same time result in higher capacity due to the increased normal stress.

5.3. Spatial analysis

In this section, the results of the numerical analysis where the spatial variation of the random variables throughout the wallette is considered will be discussed. Similar to the non-spatial analysis, brick and joint failures are grouped using an automated code-based procedure. Force-displacement curves separated for brick and joint failures for all vertical stress levels can be found in Appendix (Fig. 16). The results of the spatial analyses are summarized in Table 4. It is noted that the wallette strength increases significantly with the increasing vertical stress. A substantial increase is found for the joint failure, with an 88% change between the zero and maximum vertical pressure (0.50 MPa), whereas a less pronounced effect is obtained for brick failure (40.4%). It should be noted that when all data are considered, the increase is 46.7%, which is almost the same as the increase observed in the first case where the spatial variation in the random variables was ignored (45.7%).

Regarding the variability of the load capacity, the COV values are much smaller in the case of spatial analysis compared to the non-spatial. In the case of joint failure, the COVs slightly decrease with the increasing normal stress. As mentioned earlier, brick failure displays increasing variability in the wallette capacity as the vertical pressure increases. This increase is associated with the increasing number of brick failures and the variability of the unit tensile strength. In other words, the wallette strength is affected by the variability of the brick tensile strength ($f_{t,u}$), spatially varying based on the statistical data given earlier in Table 2.

A noticeable outcome of the vertical pressure is a change in the number of failure modes. The relationship between the vertical stress and the percentage of the observed failure modes is plotted in Fig. 11 for the two cases where the spatial variation is ignored and considered. As depicted in the plot, the percentage of the cases failing in brick failure mode increases almost linearly with the normal stress for both cases of spatial and non-spatial variation. This trend also implies that with a further increase in vertical pressure, it may not be possible to observe joint failures anymore. It is worth recalling that brick failure includes brick cracking followed by joint separation. The total number of joint and brick failures is 330 and 170, respectively, in the case of the non-spatial analysis. On the other hand, the spatial analysis has 258 joint failures and 242 brick failures.

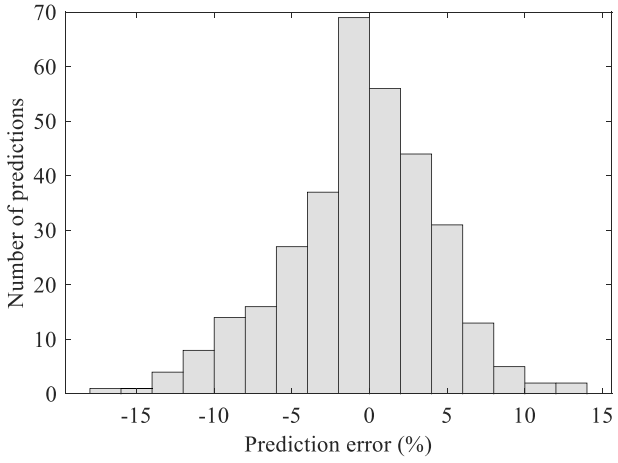

Fig. 13. Prediction error for *joint failure*.

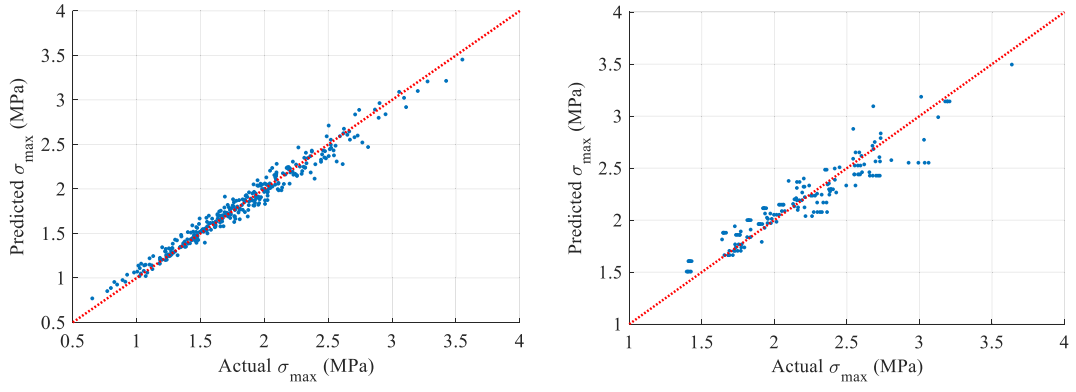

Fig. 12. Comparison of maximum stresses obtained from DEM and Equation 10: (a) DEM vs. Equation 10a; DEM vs. Equation 10b.

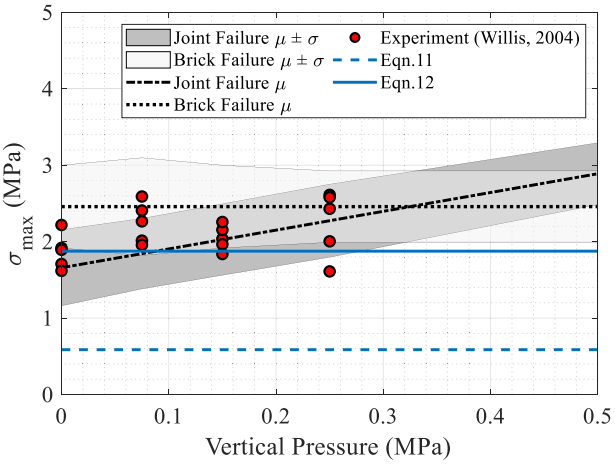

a) Comparison of the experiments, proposed and recommended strength prediction equations (Eqn 11-12, [66]).

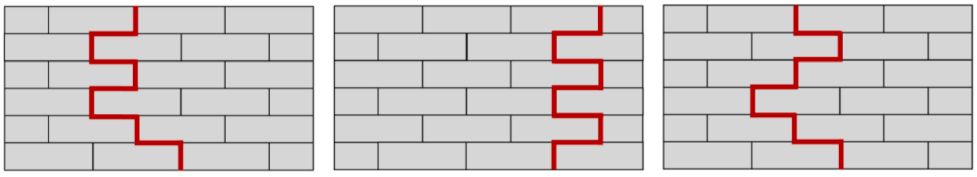

b) Illustration of joint failure patterns based on experimental results [68].

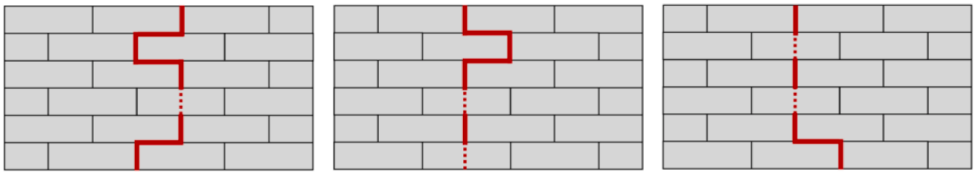

c) Illustration of brick failure based on experimental results [68].

Fig. 14. Comparison of the experimental results [69] against the proposed formula (Equation 10a-b).

6. Prediction of wallette strength

After classifying the failure types and the effect of modeling parameters on the OOP capacity of the masonry wallettes, the question remains as to whether we can accurately predict the wallette strength for the given configuration and boundary conditions with limited information, *i.e.*, without conducting numerical analysis or extensive tests. The prediction can be made using parametric models such as explicit equations or non-parametric models like support vector machines (SVM) or artificial neural networks (ANN), which apply an algorithm to the data and do not have a closed-form solution. Ultimately, these prediction models can be used to estimate the OOP load-carrying capacity of the masonry wallettes. In this regard, a linear regression approach is followed using only the joint tensile strength ($f_{t,j}$), unit tensile strength ($f_{t,u}$) and the vertical pressure (σ_v) and explicit formula in terms of these predictor variables is provided. These parameters are relatively easier to obtain in a standard construction materials laboratory. On the other hand, obtaining the elasticity modulus of bricks (E_b) and joint friction angle (ϕ) requires more effort and a complex experimental setup.

Linear regression is one of the simplest and most commonly used regression techniques. The response is modeled as an explicit equation in terms of the predictor variables and for an input vector of $x = (x_1, x_2, \cdots, x_p)$, the real-valued response y is estimated. A linear regression model has the form given in Equation 5.

$$f(x) = w_0 + \sum_{j=1}^{p} w_j x_j \tag{5}$$

Here, w_j are the coefficients (or unknown parameters) of the model and p is the number of input parameters. The coefficients of the model are estimated using a set of predictor variables and response data, *i.e.*, $(x_1, y_1), \cdots, (x_n, y_n)$. Each $x_i = (x_{i1}, x_{i2}, \cdots, x_{ip})$ is a vector of predictor variables for the i^{th} case. The estimation is often performed by using *least squares,* in which the coefficients (w_j) are selected to minimize the residual squared error or the residual sum of squares (RSS) [72].

$$RSS(w) = \sum_{i}^{n} (y_i - f(x_i))^2 = \sum_{i=1}^{n} \left(y_i - w_0 - \sum_{j=1}^{p} w_j x_{ij} \right)^2 \tag{6}$$

The least squares estimates often have low bias, but the large variance and small changes in data may result in a very different set of coefficients. It is possible to sacrifice a little bias by shrinking the coefficients (or setting some of them to zero) and increasing the prediction accuracy. This regularization technique is called "Least Absolute Shrinkage and Selection Operator" *(Lasso)* [73] and is used in this study to determine the coefficients of the regression model. In Lasso regression, the coefficients are shrunk by imposing a penalty on their size. Introducing the penalty term reduces the variance of the coefficients and minimizes the prediction error (RSS). The Lasso estimate is defined by Equation 7.

$$\widehat{w}^{lasso} = \underset{w}{\operatorname{argmin}} \sum_{i=1}^{n} \left(y_i - w_0 - \sum_{j=1}^{p} w_j x_{ij} \right)^2$$

$$\text{subject to} \sum_{j=1}^{p} |w_j| \le t \tag{7}$$

Equation 7 can be written in the equivalent Lagrangian form, as

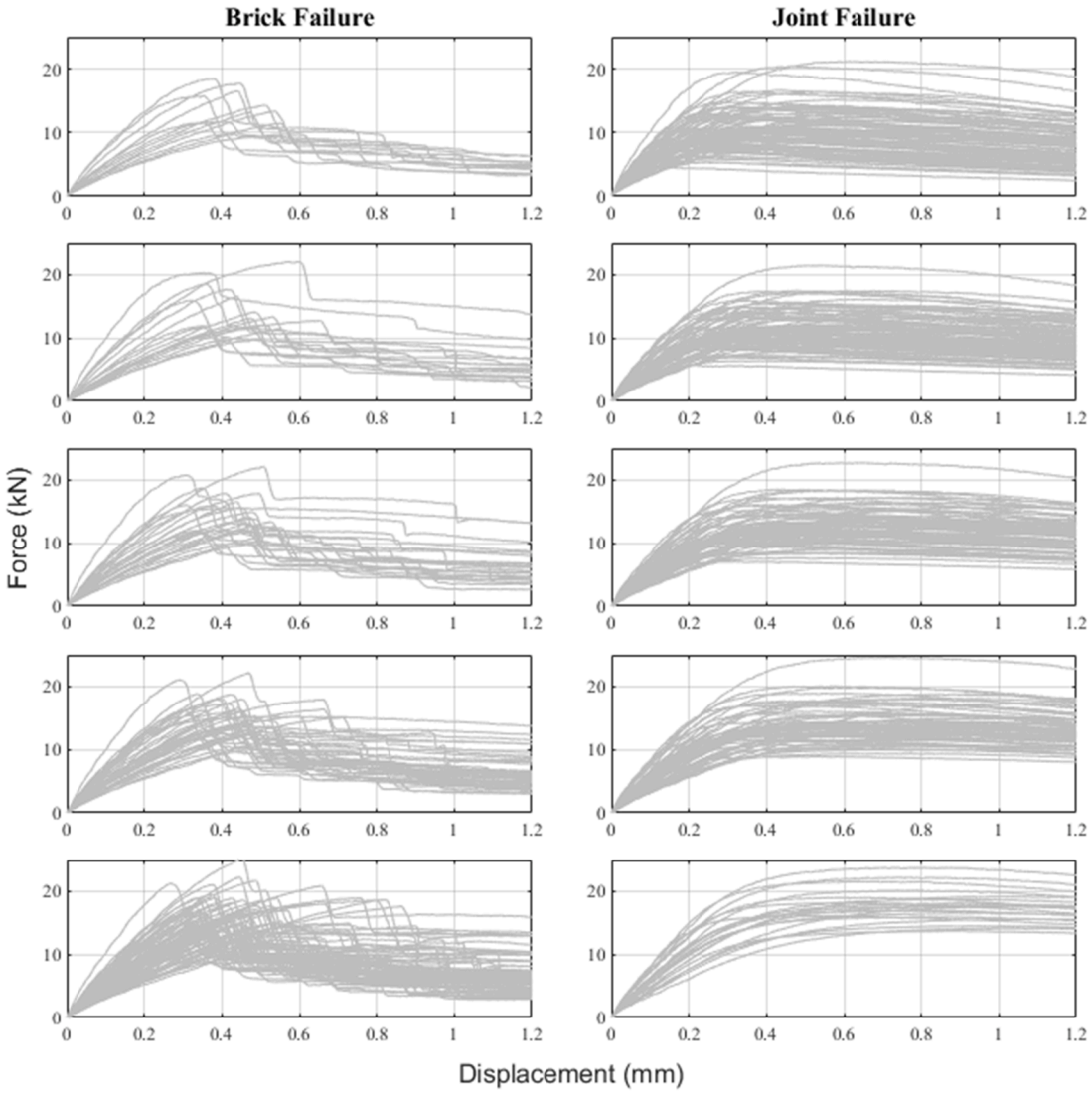

Fig. 15. Force-displacement curves for non-spatial analyses: brick failure (left) and joint failure (right) when the vertical pressure is 0 (top) and 0.5 MPa (bottom).

follows:

$$\widehat{w}^{lasso} = \underset{w}{\operatorname{argmin}} \left\{ \frac{1}{2} \sum_{i=1}^{n} (y_i - w_0 - \sum_{j=1}^{p} w_j x_{ij})^2 + \lambda \sum_{j=1}^{p} |w_j| \right\} \tag{8}$$

where $\lambda \geq 0$ is a tuning parameter and controls the amount of shrinkage applied to the estimates. The larger the values of λ, the greater the shrinkage of the coefficients toward zero. Note that a one-to-one correspondence exists between the parameters t and λ, given in Equations 7 and 8 [72]. The Lasso regression imposes the penalty term on the l_1 norm of the coefficients. Because of the form of the Lasso penalty, the coefficients of the insignificant variables shrink to zero while the most significant variables are retained, *i.e.*, there is automatic variable selection [74].

In this study, Lasso regression is carried out to obtain the response estimates $\widehat{y}$ using the predictor variables $x = (f_{t,u}, f_{t,j}, {f_{t,u}}^2, {f_{t,j}}^2, \sigma_v)$. The dataset from the non-spatial analysis only is used as this approach represents a real-world application better. The value of the lambda parameter is determined by observing the changes in the mean square error (MSE) given in Equation 9. Five-fold cross-validation is applied to assess and improve the predictive performance of the regression model. In each round of cross-validation, the dataset is partitioned into a *training set* and a *test set*. In this case, the dataset is divided into five randomly chosen subsets of roughly equal size. Four subsets are used to train the model, while the remaining subset is used to validate the trained model. This process is repeated five times until all subsets are used once to test the model. The readers are referred to Hastie et al. [72] for further information on the cross-validation techniques.

$$MSE = \frac{1}{n} \sum_{i=1}^{n} (y - \widehat{y})^2 \tag{9}$$

The data sets of brick and joint failures are used separately in Lasso regression to obtain the coefficients and the intercepts of the linear regression equations. Consequently, two formulas, one for each failure mode, are given in Equation 10. Equations 10a and 10b predict the wallette strength (in MPa) for *joint* and *brick failures*, respectively. Here, it should be noted that the forces are converted to bending stresses using $\sigma = 6M/(bh^2)$, as strength is represented in terms of stress capacity, in line with [67] and engineering applications. The moment generated by lateral loading is $M = 0.1375 \bullet P$ (in kN.m), base is $b = 0.44$ m and height h = 0.114 m. The maximum stress obtained from the computational models and the predictions made by Equation 10 are compared in Fig. 12. The prediction error is calculated in terms of its absolute value and ratio (%) to the response value, presented in Fig. 13. The figure shows that most predictions are in the range of ± 10% of the response values. Also, the mean average prediction percentage (MAPE) error is 3.71 %.

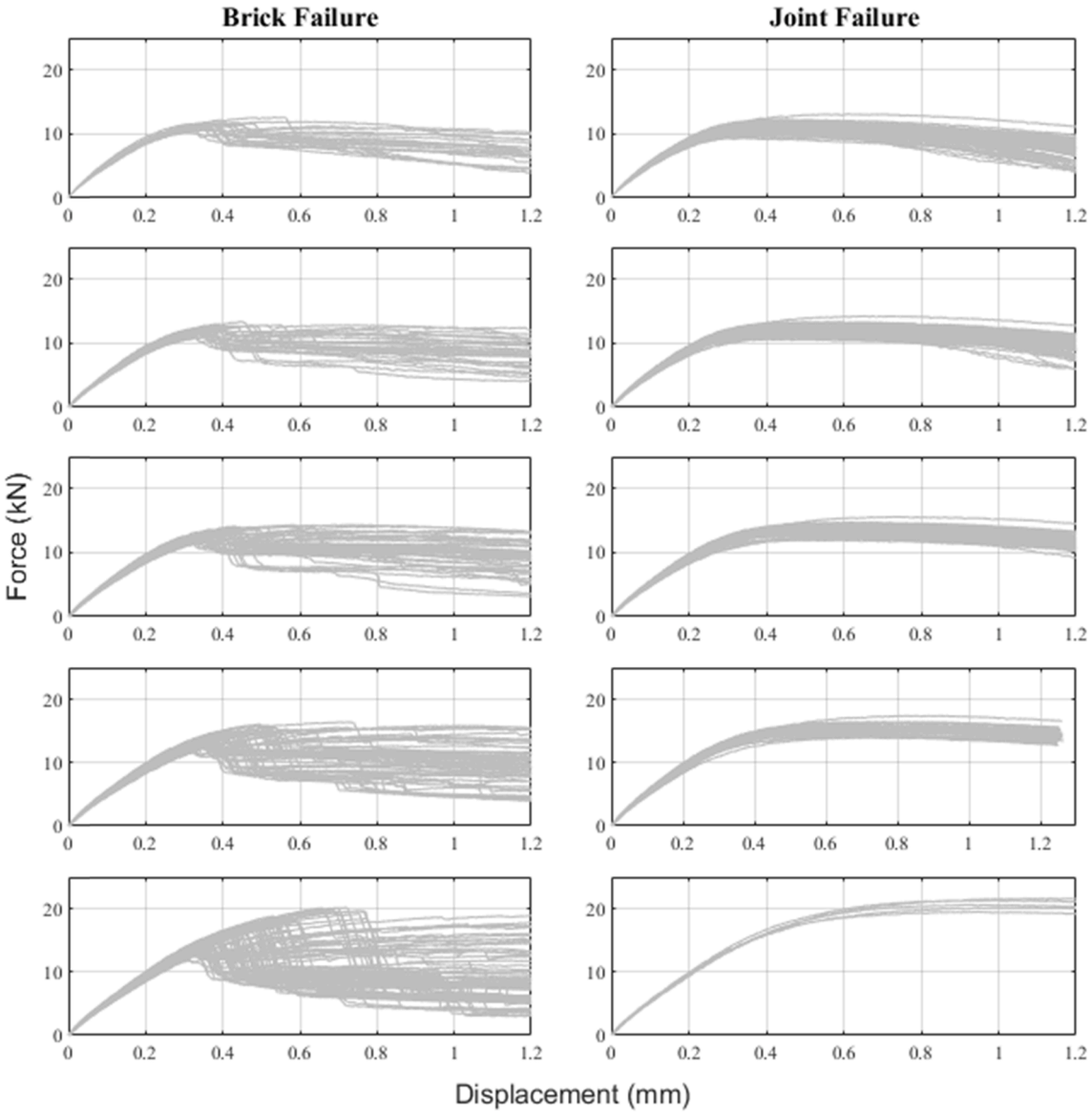

Fig. 16. Force-displacement curves for spatial analyses: brick failures (left) and joint failures (right) when the vertical pressure is 0 (top) to 0.5 MPa (bottom).

$$\sigma_{JF} = 0.24 + 0.017 f_{t,u} + 4.515 f_{t,j} + 2.46\sigma_v \tag{10a}$$

$$\sigma_{BF} = 0.53 + 0.50 f_{t,u} + 0.176 f_{t,j} \tag{10b}$$

Only *apriori* information about the values of the predictor variables is required to predict the wallette strength, which will be the lesser of the two estimates. In other words, to estimate the failure type and wallette strength, Equations 10a and 10b are used, and the lower value is taken as the wallette capacity in horizontal bending. The failure type will be associated with the lower strength estimate. This approach is applied, and the results obtained from Equation 10 are compared to the experimental findings presented by Willis [69], as shown in Fig. 14. The proposed equations for joint and brick failure modes are plotted considering the mean values of $f_{t,j}$ and $f_{t,u}$ given in Table 2. Therefore, only one deterministic value for each of these two variables is taken, and these values can practically be the mean values obtained from the relatively simple component tests of masonry. To better evaluate the comparison of test and prediction values, the standard deviations in Table 3 for the force capacity are used to offset the mean prediction values and plot the shaded regions in between.

Additionally, two lower-bound tensile strength formulations for a masonry wallette ($f_{t,M}$) subjected to tension parallel to bed joints, recommended in [67], are compared against the experimental results and proposed expressions. The first formula corresponds to the stepped cracking or joint failure (Equation 11) in the absence of vertical pressure; hence it gives conservative predictions, whereas the second one is related to the brick failure (Equation 12), assuming the masonry tensile strength equal to half of the unit tensile strength.

$$f_{t,M} = \frac{c_j l_o}{h_b} \tag{11}$$

where, l_o and h_b are the units overlapping length and unit height, respectively.

$$f_{t,M} = \frac{f_{t,u}}{2} \tag{12}$$

An important observation is that the provided equations predict conservatively compared to the experiments. Also, all test results fall within the predicted regions except for one outlier. Compared with the experimental results, a similar number of bricks and joint failures are observed. An inverse comparison is carried out, predicting the strength values for the observed failure modes. In other words, the experimental

strength values are similar to the predicted capacities for the same failure modes observed in the tests. Fig. 14(b) and 14(c) show failure patterns observed in the experimental campaign. It should be noted that the vertical stress levels are extrapolated in the computational models to account for various scenarios; however, [69] does not include experimental results for higher levels of normal stress, such as 0.50 MPa.

It is worth noting that the proposed expressions (Equation 10) are limited to the given range of parameter values, unit types, and geometrical proportions; however, the authors would like to display the potential of the proposed framework that can be modified, including additional parameters for general relevance, such as the geometry of the brick. A key finding of this study highlights the most important input parameters on the out-of-plane bending response of masonry wallettes, which play a foundation role in future studies to propose a more general formula.

7. Conclusions

This study proposes a novel approach to generate data for the statistical learning algorithms to predict the failure mode and capacity of complex masonry systems by using less complicated and inexpensive test results and an advanced discontinuum-based modeling strategy. Masonry wallettes subjected to out-of-plane horizontal bending are analyzed using discrete element models incorporating elasto-plastic blocks interacting with each other along their boundaries. The adopted modeling technique provides detailed information regarding the shear and coupled tension-shear behavior of the unit-mortar interface. The DEM-based model, which is first validated using experimental data, is utilized to perform stochastic analysis, implementing the material uncertainties.

Throughout the study, the importance of implementing the variability in mechanical properties of the masonry is demonstrated. The results contribute to the knowledge in quantifying the variability of the wallette capacity and the effects of the material parameters on the failure mechanism and strength of the masonry wallettes. They also show that the most critical parameters changing the response are the joint tensile strength and the amount of normal stress for *joint failure*, whereas the unit tensile strength dominates the response in the *brick failure* condition. The spatial variation of modeling properties is also taken into account in the spatial stochastic analysis, and the results are compared to the non-spatial case where each parameter has a single value for the entire wallette. The stochastic analysis with spatial variability generally resulted in lower variation in the wallette capacity, complying with the existing literature. However, different from the previous findings, it is noticed that this trend is also failure-mode dependent. The coefficient of variation of the wallette capacity increases for the higher levels of vertical pressure as the number of brick failures increase significantly.

Furthermore, a data set generated by stochastic computational simulations is used to develop prediction models for the load-bearing capacity of the wallette for the different failure types. A good agreement is observed between the predictions and the experimental results obtained from the literature. Overall, it is demonstrated that the prediction of the capacity and behavior of masonry structures using advanced stochastic discontinuum-based models, fed by experimental data obtained on smaller structural scales, promises great potential for research and practice.

The application of the proposed approach should be extended to include various configurations, materials, typology, geometry, and boundary conditions. The future work will investigate the application of the proposed methodology to the standardized masonry tests on components.

CRediT authorship contribution statement

Semih Gonen: Conceptualization, Methodology, Software, Validation, Formal analysis, Visualization, Writing – original draft, Writing – review & editing. **Bora Pulatsu:** Conceptualization, Methodology, Software, Validation, Formal analysis, Visualization, Writing – original draft, Writing – review & editing. **Paulo B. Lourenço:** Methodology, Writing – review & editing. **José V. Lemos:** Methodology, Writing – review & editing. **Kagan Tuncay:** Methodology, Writing – review & editing. **Emrah Erduran:** Writing – review & editing.

Declaration of Competing Interest

The authors declare that they have no known competing financial interests or personal relationships that could have appeared to influence the work reported in this paper.

Data availability

Data will be made available on request.

Appendix

See Figs. 15-16.

References

[1] Ortega J, Vasconcelos G, Rodrigues H, Correia M. Assessment of the efficiency of traditional earthquake resistant techniques for vernacular architecture. Eng Struct 2018;173:1–27. https://doi.org/10.1016/j.engstruct.2018.06.101.

[2] Gönen S, Liebhart RF, Miller NF, Dusinberre ERM. Archaeology and conservation of the middle phrygian gate complex at Gordion, Turkey. Bull Am Sch Orient Res 2018;379:55–85. https://doi.org/10.5615/bullamerschoorie.379.0055.

[3] Pulatsu B, Gonen S, Erdogmus E, Lourenço PB, Lemos JV, Hazzard J. Tensile Fracture Mechanism of Masonry Wallettes Parallel to Bed Joints: A Stochastic Discontinuum Analysis. Model Open Access J Model Eng Sci 2020;1:78–93. https://doi.org/10.3390/modelling1020006.

[4] Godio M, Vanin F, Zhang S, Beyer K. Quasi-static shear-compression tests on stone masonry walls with plaster: Influence of load history and axial load ratio. Eng Struct 2019;192:264–78. https://doi.org/10.1016/j.engstruct.2019.04.041.

[5] Roca P, Cervera M, Gariup G, Pela' L. Structural Analysis of Masonry Historical Constructions. Classical and Advanced Approaches. Arch Comput Methods Eng 2010;17:299–325. https://doi.org/10.1007/s11831-010-9046-1.

[6] Lourenço PB, Rots JG, Blaauwendraad J. Continuum Model for Masonry: Parameter Estimation and Validation. J Struct Eng 1998;124:642–52. https://doi.org/10.1061/(ASCE)0733-9445(1998)124:6(642).

[7] Saloustros S, Pelà L, Roca P, Portal J. Numerical analysis of structural damage in the church of the Poblet Monastery. Eng Fail Anal 2015;48:41–61. https://doi.org/10.1016/j.engfailanal.2014.10.015.

[8] Aldemir A, Erberik MA, Demirel IO, Sucuoglu H. Seismic performance assessment of unreinforced masonry buildings with a hybrid modeling approach. Earthq Spectra 2013;29:33–57. https://doi.org/10.1193/1.4000102.

[9] Sesigur H, Erol G, Soyoz S, Kaynardag K, Gonen S. Repair and retrofit of Ketchaoua Mosque in Algeria. Struct. Anal. Hist. Constr. Anamn. diagnosis, ther, controls. - Proc. 10th Int. Conf. Struct. Anal. Hist. Constr. SAHC 2016;2016:1824–31. https://doi.org/10.1201/9781315616995-267.

[10] Demirlioglu K, Gonen S, Soyoz S, Limongelli MP. In-Plane Seismic Response Analyses of a Historical Brick Masonry Building Using Equivalent Frame and 3D FEM Modeling Approaches. Int J Archit Herit 2020;14:238–56. https://doi.org/10.1080/15583058.2018.1529208.

[11] Lourenço PB. Computational strategies for masonry structures. Delft University of Technology; 1996.

[12] Demirel IO, Aldemir A. Simplified Approach for Seismic Performance Assessment of Dry-Joint Masonry Arch Bridges. Buildings 2021;11(7):313. https://doi.org/10.3390/buildings11070313.

[13] Andreotti G, Graziotti F, Magenes G. Detailed micro-modelling of the direct shear tests of brick masonry specimens: The role of dilatancy. Eng Struct 2018;168:929–49. https://doi.org/10.1016/j.engstruct.2018.05.019.

[14] Bisoffi-Sauve M, Morel S, Dubois F. Modelling mixed mode fracture of mortar joints in masonry buildings. Eng Struct 2019;182:316–30. https://doi.org/10.1016/j.engstruct.2018.11.064.

[15] Lemos JV, Sarhosis V. Discrete Element Bonded-Block Models for Detailed Analysis of Masonry. Infrastructures 2022;7:31. https://doi.org/10.3390/infrastructures7030031.

[16] Pulatsu B, Erdogmus E, Lourenço PB, Lemos JV, Hazzard J. Discontinuum analysis of the fracture mechanism in masonry prisms and wallettes via discrete element method. Meccanica 2020;55:505–23. https://doi.org/10.1007/s11012-020-01133-1.

[17] Pulatsu B, Erdogmus E, Lourenço PB, Quey R. Simulation of uniaxial tensile behavior of quasi-brittle materials using softening contact models in DEM. Int J Fract 2019;217:105–25. https://doi.org/10.1007/s10704-019-00373-x.

[18] Pascuzzo A, Greco F, Leonetti L, Lonetti P, Ronchei C, Gaetano D. An interface-based detailed micro-model for the failure simulation of masonry structures. Eng Fail Anal 2022;142:106753. https://doi.org/10.1016/j.engfailanal.2022.106753.

[19] Patel KP, Dubey RN. Effect of flanges on the in-plane behavior of the masonry walls. Eng Struct 2022;273:115059. https://doi.org/10.1016/j.engstruct.2022.115059.

[20] Zhang S, Beyer K. Numerical investigation of the role of masonry typology on shear strength. Eng Struct 2019;192:86–102. https://doi.org/10.1016/j.engstruct.2019.04.026.

[21] Godio M, Stefanou I, Sab K, Sulem J, Sakji S. A limit analysis approach based on Cosserat continuum for the evaluation of the in-plane strength of discrete media: Application to masonry. Eur J Mech - A/Solids 2017;66:168–92. https://doi.org/10.1016/J.EUROMECHSOL.2017.06.011.

[22] Malomo D, DeJong MJ. M-DEM simulation of seismic pounding between adjacent masonry structures. Bull Earthq Eng 2022. https://doi.org/10.1007/s10518-022-01545-2.

[23] Gonen S, Pulatsu B, Erdogmus E, Karaesmen E, Karaesmen E. Quasi-static nonlinear seismic assessment of a fourth century AD Roman aqueduct in Istanbul, Turkey. Heritage 2021;4:401–21. https://doi.org/10.3390/heritage4010025.

[24] Gonen S, Pulatsu B, Soyoz S, Erdogmus E. Stochastic discontinuum analysis of unreinforced masonry walls: Lateral capacity and performance assessments. Eng Struct 2021;238:112175. https://doi.org/10.1016/j.engstruct.2021.112175.

[25] Gonen S, Pulatsu B, Erdogmus E, Lourenço PB, Soyoz S. Effects of spatial variability and correlation in stochastic discontinuum analysis of unreinforced masonry walls. Constr Build Mater 2022;337:127511. https://doi.org/10.1016/j.conbuildmat.2022.127511.

[26] Pulatsu B, Erdogmus E, Bretas EM, Lourenço PB. In-Plane Static Response of Dry-Joint Masonry Arch-Pier Structures. AEI 2019, Reston, VA: American Society of Civil Engineers; 2019, p. 240–8. https://doi.org/10.1061/9780784482261.028.

[27] Li J, Masia MJ, Stewart MG, Lawrence SJ. Spatial variability and stochastic strength prediction of unreinforced masonry walls in vertical bending. Eng Struct 2014;59:787–97. https://doi.org/10.1016/j.engstruct.2013.11.031.

[28] Li J, Masia MJ, Stewart MG. Stochastic spatial modelling of material properties and structural strength of unreinforced masonry in two-way bending. Struct Infrastruct Eng 2017;13:683–95. https://doi.org/10.1080/15732479.2016.1188125.

[29] Müller D, Förster V, Graubner C-A. Influence of material spatial variability on required safety factors for masonry walls in compression. Mauerwerk 2017;21:209–22. https://doi.org/10.1002/dama.201700004.

[30] Isfeld AC, Stewart MG, Masia MJ. Stochastic finite element model assessing length effect for unreinforced masonry walls subjected to one-way vertical bending under out-of-plane loading. Eng Struct 2021;236. https://doi.org/10.1016/j.engstruct.2021.112115.

[31] Gooch LJ, Masia MJ, Stewart MG. Application of stochastic numerical analyses in the assessment of spatially variable unreinforced masonry walls subjected to in-plane shear loading. Eng Struct 2021;235. https://doi.org/10.1016/j.engstruct.2021.112095.

[32] Howlader MK, Masia MJ, Griffith MC. Numerical analysis and parametric study of unreinforced masonry walls with arch openings under lateral in-plane loading. Eng Struct 2020;208:110337. https://doi.org/10.1016/j.engstruct.2020.110337.

[33] Pulatsu B, Gonen S, Parisi F, Erdogmus E, Tuncay K, Funari MF, et al. Probabilistic approach to assess URM walls with openings using discrete rigid block analysis (D-RBA). J Build Eng 2022;61:105269. https://doi.org/10.1016/j.jobe.2022.105269.

[34] Parisi F, Augenti N. Uncertainty in Seismic Capacity of Masonry Buildings. Buildings 2012;2:218–30. https://doi.org/10.3390/buildings2030218.

[35] Erberik MA. Generation of fragility curves for Turkish masonry buildings considering in-plane failure modes. Earthq Eng Struct Dyn 2008;37:387–405. https://doi.org/10.1002/eqe.760.

[36] Bosiljkov V, D'Ayala D, Novelli V. Evaluation of uncertainties in determining the seismic vulnerability of historic masonry buildings in Slovenia: use of macro-element and structural element modelling. Bull Earthq Eng 2015;13:311–29. https://doi.org/10.1007/s10518-014-9652-7.

[37] Gönen S, Soyöz S. Reliability-based seismic performance of masonry arch bridges. Struct Infrastruct Eng 2021:1–16. https://doi.org/10.1080/15732479.2021.1918726.

[38] Jahangiri V, Yazdani M. Seismic reliability and limit state risk evaluation of plain concrete arch bridges. Struct Infrastruct Eng 2021;17:170–90. https://doi.org/10.1080/15732479.2020.1733030.

[39] Jiménez Rios A, Nela B, Pingaro M, Reccia E, Trovalusci P. Rotation and sliding collapse mechanisms for in plane masonry pointed arches: statistical parametric assessment. Eng Struct 2022;262:114338. https://doi.org/10.1016/J.ENGSTRUCT.2022.114338.

[40] Sharma S, Graziotti F, Magenes G. Torsional shear strength of unreinforced brick masonry bed joints. Constr Build Mater 2021;275:122053. https://doi.org/10.1016/j.conbuildmat.2020.122053.

[41] Lourenço PB, Rots JG, Van der Pluijm R. Understanding the Tensile Behavior of Masonry Parallel to the Bed Joints- A Numerical Approach. Mason Int 1999;12:96–103.

[42] Willis C, Griffith M, Lawrence S. Horizontal bending of unreinforced clay bricks. Mason Int 2004;17:109–21.

[43] Cox FW, Ennenga JL. Transverse Strength of Concrete Block Walls. J Am Concr Inst 1958;54:951–60.

[44] Ardito R, Taliercio A. Flexural capacity of long-span transversely loaded hollow block masonry walls. Constr Build Mater 2019;220:489–502. https://doi.org/10.1016/j.conbuildmat.2019.06.042.

[45] Asteris PG, Lourenço PB, Hajihassani M, Adami CEN, Lemonis ME, Skentou AD, et al. Soft computing-based models for the prediction of masonry compressive strength. Eng Struct 2021;248:113276. https://doi.org/10.1016/j.engstruct.2021.113276.

[46] Ferretti D. Dimensional analysis and calibration of a power model for compressive strength of solid-clay-brick masonry. Eng Struct 2020;205:110064. https://doi.org/10.1016/j.engstruct.2019.110064.

[47] Lan G, Wang Y, Zeng G, Zhang J. Compressive strength of earth block masonry: Estimation based on neural networks and adaptive network-based fuzzy inference system. Compos Struct 2020;235:111731. https://doi.org/10.1016/j.compstruct.2019.111731.

[48] Mishra M, Bhatia AS, Maity D. Predicting the compressive strength of unreinforced brick masonry using machine learning techniques validated on a case study of a museum through nondestructive testing. J Civ Struct Heal Monit 2020;10:389–403. https://doi.org/10.1007/s13349-020-00391-7.

[49] Müller D, Graubner C-A. Assessment of Masonry Compressive Strength in Existing Structures Using a Bayesian Method. ASCE-ASME J Risk Uncertain Eng Syst Part A Civ Eng 2021;7:04020057. https://doi.org/10.1061/ajrua6.0001113.

[50] Gholami M, Gholami A. Prediction of compressive strength of masonry structures : Integrating three optimized models by virtue of committee machine. Structures 2022;44:1127–37. https://doi.org/10.1016/j.istruc.2022.08.079.

[51] Mishra M. Machine learning techniques for structural health monitoring of heritage buildings: A state-of-the-art review and case studies. J Cult Herit 2021;47:227–45. https://doi.org/10.1016/j.culher.2020.09.005.

[52] Cundall PA. A computer model for simulating progressive, large-scale movements in blocky rock systems. Int. Symp. Rock Mech., vol. 2, Nancy: 1971, p. 47–65.

[53] Lourenço PB. Computations on historic masonry structures. Prog Struct Eng Mater 2002;4:301–19. https://doi.org/10.1002/pse.120.

[54] Cundall P, Detournay C. Dynamic relaxation applied to continuum and discontinuum numerical models in geomechanics. Rock Mech Eng Vol 3 Anal Model Des 2017:45–90. https://doi.org/10.1201/b20402.

[55] Pulatsu B, Erdogmus E, Lourenço PB, Lemos JV, Tuncay K. Simulation of the in-plane structural behavior of unreinforced masonry walls and buildings using DEM. Structures 2020;27:2274–87. https://doi.org/10.1016/j.istruc.2020.08.026.

[56] Marti J, Cundall PA. Mixed Discretization Procedure for Accurate Solution of Plasticity Problems. Int J Numer Anal Methods Geomechanics 1982;6:129–39.

[57] Detournay C, Dzik E. Nodal Mixed Discretization for tetrahedral elements. 4th Int FLAC Symp Numer Model Geomech 2006;c:07–02.

[58] Itasca Consulting Group Inc. 3DEC Three Dimensional Distinct Element Code 2013.

[59] Pulatsu B, Gonen S, Erdogmus E, Lourenço PB, Lemos JV, Prakash R. In-plane structural performance of dry-joint stone masonry Walls: A spatial and non-spatial stochastic discontinuum analysis. Eng Struct 2021;242:112620. https://doi.org/10.1016/j.engstruct.2021.112620.

[60] Lemos JV. Block modelling of rock masses. Concepts and application to dam foundations. Rev Eur Génie Civ 2008;12:915–49. https://doi.org/10.3166/ejece.12.915-949.

[61] Willis RC, Griffith MC, Lawrence S. Horizontal Bending of Unreinforced Clay Brick Masonry. Mason Int 2005;8:125–38.

[62] Lourenço PB, Oliveira DV, Roca P, Orduña A. Dry Joint Stone Masonry Walls Subjected to In-Plane Combined Loading. J Struct Eng 2005;131:1665–73. https://doi.org/10.1061/(ASCE)0733-9445(2005)131:11(1665).

[63] Gonen S, Soyoz S. Investigations on the elasticity modulus of stone masonry. Structures 2021;30:378–89. https://doi.org/10.1016/j.istruc.2021.01.035.

[64] Vanmarcke E, Shinozuka M, Nakagiri S, Schuëller GI, Grigoriu M. Random fields and stochastic finite elements. Struct Saf 1986;3:143–66. https://doi.org/10.1016/0167-4730(86)90002-0.

[65] Lourenço PB. Recent advances in masonry structures: Micromodelling and homogenisation, in: Multiscale Modeling in Solid Mechanics: Computational Approaches. Multiscale Model. solid Mech. Comput. approaches, 2009, p. 251–94.

[66] Jafari S, Rots JG, Esposito R. A correlation study to support material characterisation of typical Dutch masonry structures. J Build Eng 2021;45:103450. https://doi.org/10.1016/j.jobe.2021.103450.

[67] Lourenço PB, Gaetani A. Recommended properties for advanced numerical analysis. Finite Elem Anal Build Assess Adv Use Pract Recomm, Routledge 2022:209–321. https://doi.org/10.31201/9780429341564-4.

[68] Li J, Stewart MG, Masia MJ, Lawrence SJ. Spatial Correlation of Material Properties and Structural Strength of Masonry in Horizontal Bending. J Struct Eng 2016;142:04016112. https://doi.org/10.1061/(asce)st.1943-541x.0001488.

[69] Willis CR. Design of Unreinforced Masonry Walls for Out-of-plane Loading. The University of Adelaide; 2004.

[70] Stewart M, Heffler L. Statistical Analysis and Spatial Correlation of Flexural Bond Strength for Masonry Walls. Mason Int 2008;21:57–70.

[71] Stein M. Large sample properties of simulations using latin hypercube sampling. Technometrics 1987;29:143–51. https://doi.org/10.1080/00401706.1987.10488205.

[72] Hastie T, Friedman J, Tibshirani R. The Elements of Statistical Learning. New York, NY: Springer New York; 2001. https://doi.org/10.1007/978-0-387-21606-5.

[73] Tibshirani R. Regression Shrinkage and Selection Via the Lasso. J R Stat Soc Ser B 1996;58:267–88. https://doi.org/10.1111/j.2517-6161.1996.tb02080.x.

[74] Mangalathu S, Jeon JS, DesRoches R. Critical uncertainty parameters influencing seismic performance of bridges using Lasso regression. Earthq Eng Struct Dyn 2018;47:784–801. https://doi.org/10.1002/eqe.2991.